Science Advances
AAAS

advances.sciencemag.org/cgi/content/full/6/15/eaax6212/DC1

Supplementary Materials for

Computational wrapping: A universal method to wrap 3D-curved surfaces with nonstretchable materials for conformal devices

Yu-Ki Lee, Zhonghua Xi, Young-Joo Lee, Yun-Hyeong Kim, Yue Hao, Hongjin Choi, Myoung-Gyu Lee, Young-Chang Joo, Changsoon Kim, Jyh-Ming Lien*, In-Suk Choi*

*Corresponding author. Email: jmlien@cs.gmu.edu (J.-M.L.); insukchoi@snu.ac.kr (I.-S.C.)

Published 10 April 2020, *Sci. Adv.* **6**, eaax6212 (2020)
DOI: 10.1126/sciadv.aax6212

The PDF file includes:

Other Supplementary Material for this manuscript includes the following:

(available at advances.sciencemag.org/cgi/content/full/6/15/eaax6212/DC1)

Supplementary Figures

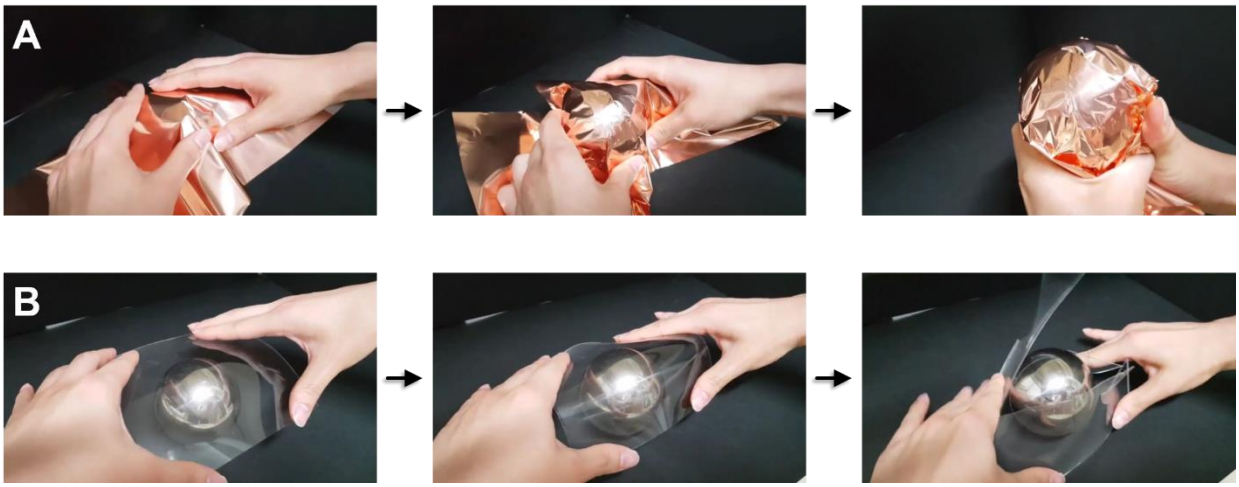

Fig. S1. Failure to cover a sphere with nonstretchable sheets. (A) Wrapping a sphere with a rectangular 30 μm-thick Cu foil inevitably forms wrinkles, crumples and overlaps. **(B)** A rectangular flexible glass substrate of a commercial liquid crystal display (LCD) panel breaks when wrapped around a sphere (See also Movie S1). (Photo credit: Y.-K. Lee, Seoul National University)

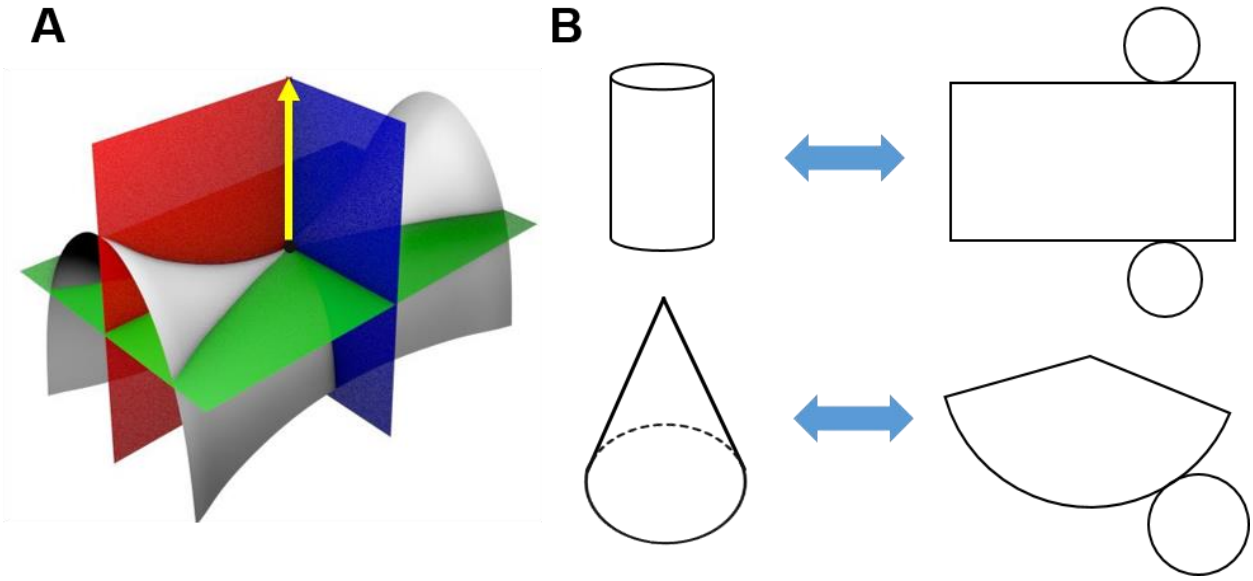

Fig. S2. Mathematical limitation of wrapping a planar sheet around a 3D surface with nonzero Gaussian curvatures. (A) Gaussian curvature is the vector product of the maximum and minimum principal curvatures at a point. At the saddle point (black dot) of the gray surface, one of the principal curvatures is the intersection between the red and gray surfaces, and the other is the intersection between the blue and gray surfaces. Both the red and blue planes contain the normal vector of the saddle point, and their intersections with the gray surface define the principal curvatures. A 2D material with zero Gaussian curvature points, such as a sheet of paper, is called a "developable surface", which cannot be transformed into a 3D surface with a positive or negative Gaussian curvature (i.e., a "nondevelopable surface") without stretching or compressing. **(B)** For example, a cylinder or a cone can be covered with cut paper, but a saddle or a sphere cannot be wrapped without the formation of wrinkles or cuts. The reverse (flattening) process is also the same, which is why there are distortions in the planar map of the Earth.

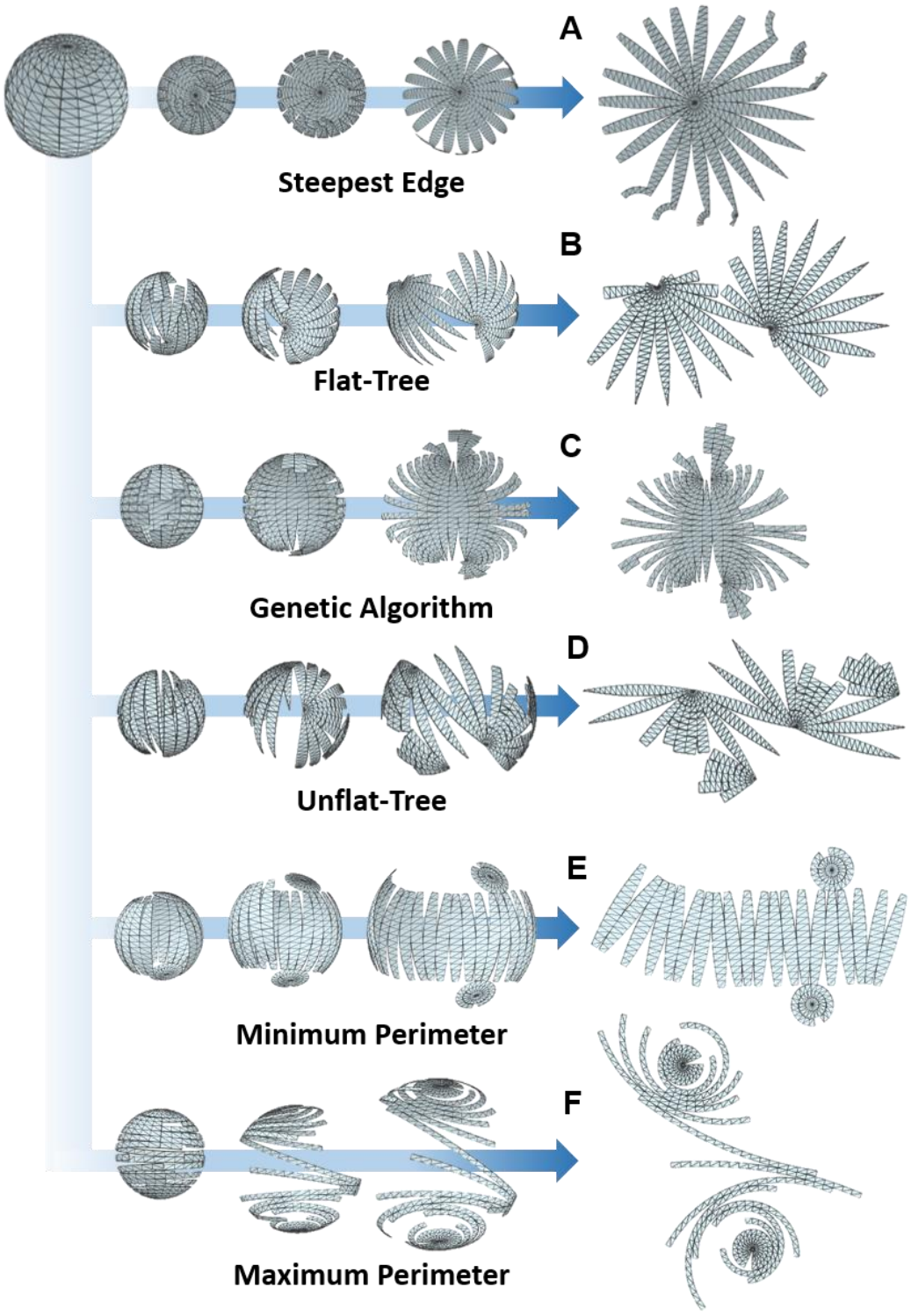

Fig. S3. Diverse mesh unfolding methods: (A) Steepest edge (SE) unfolding; **(B)** Flat-Tree unfolding; **(C)** unfolding obtained by the proposed Genetic Algorithm, which is optimized to reduce the cut length; **(D)** Unflat-Tree unfolding, in which the edge weight w'_i is equal to $w'_i = 1 - w_i$, where w_i is the edge weight used in Flat-Tree unfolding; **(E)** minimum perimeter; and **(F)** maximum perimeter.

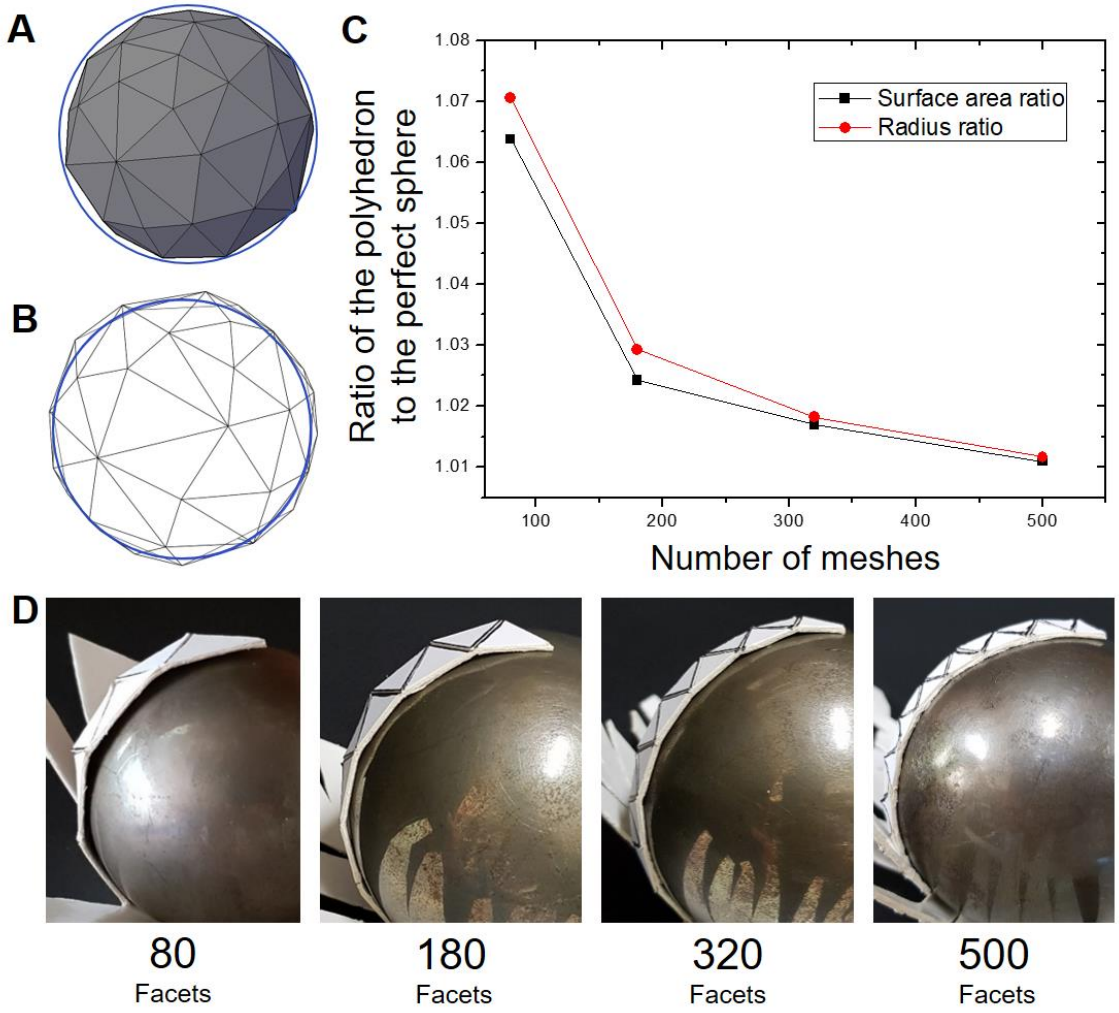

Fig. S4. Polyhedral spheres that bound the perfect sphere with different numbers of meshes. A polyhedral sphere is generated by meshing a perfect sphere with different mesh numbers. The polyhedral sphere is then scaled to enclose the perfect sphere while minimizing the Hausdorff distance. **(A)** For example, 80 meshes are used to make a polyhedron sphere out of a perfect sphere (blue solid line), and then the scaled-up polyhedron is illustrated in **(B). (C)** The surface area and the scaled radius of the polyhedron decrease and approach those of the perfect sphere as the number of meshes increases. **(D)** Naturally, the folding angles between two adjacent meshes decrease as the number of meshes increases. Consequently, the minimal folding angles with a sufficiently large number of meshes can lead to a nonpolyhedral developable net for computational wrapping, wherein all the crease lines are ignored. (Photo credit: Y.-K. Lee, Seoul National University)

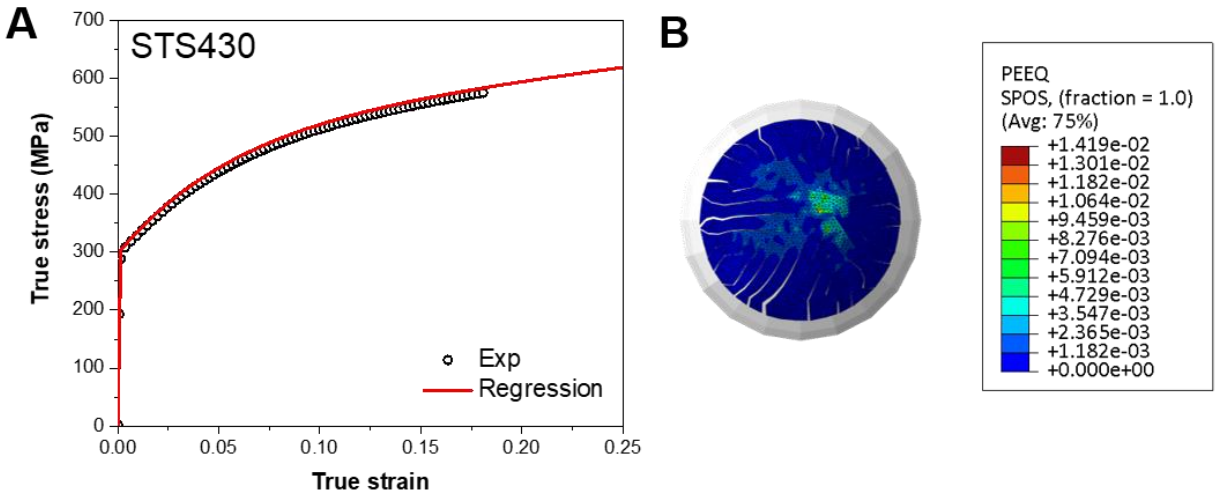

Fig. S5. Finite element analysis for wrapping a part of a sphere with a stainless steel developable net. We used an FE simulation approach similar to the Si wafer case for a 100 μm - thick stainless steel sheet. **(A)** For the stainless steel sheet, a stress-strain curve (black circular dots) is obtained through a uniaxial tensile test. For a constitutive equation of the stainless steel implemented in FE simulation, the Swift-Voce model (28, 29) is then used to fit the experimental stress-strain curve. The Swift-Voce hardening law is expressed as follows:

$$\bar{\sigma} = R(K(\varepsilon_0 + \varepsilon^p)^n) + (1 - R)\left(\sigma_s - \left(\sigma_s - \sigma_y\right)\exp(-c\varepsilon^p)\right)$$

The values obtained by fitting are R = 0.5449, $\boldsymbol{\varepsilon_0}$ = 0.018, K = 965.9 MPa, N = 0.2921, C = 16.63, σ_s = 580.0 MPa, and σ_y = 304.0 MPa. The root mean square error (RMSE) of the regression is 6.098, and R-squared is 0.9925. The elastic properties in the simulation are as follows: Young's modulus $E = 209.1$ GPa and Poisson's ratio $\nu = 0.3$. **(B)** The stress is concentrated at the sharp tips between two adjacent strips of the developable net during the wrapping process such that the equivalent plastic strain values are higher in this centered area where the tips converge. The equivalent plastic strain in the nets is mostly less than 0.005, and even the maximum value of the equivalent plastic strain in the centered area is merely 0.014. These low values of the equivalent plastic strain indicate that the computational wrapping method effectively relieves the stress evolution in the net.

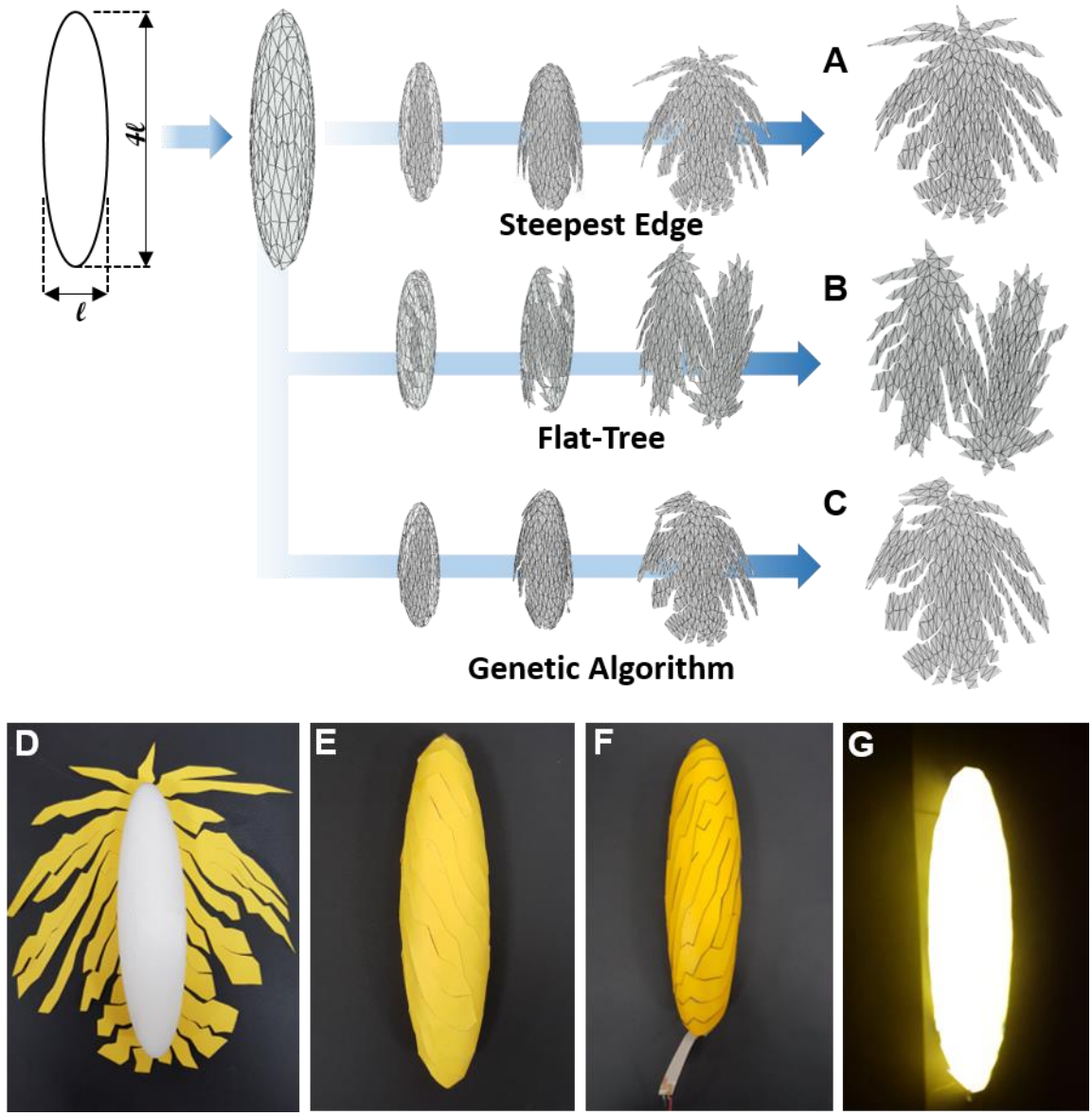

Fig. S6. Computational wrapping for an ellipsoid model. All of the points on a sphere have the same Gaussian curvature, but other solid figures with nonuniform Gaussian curvatures can also be deployed by using diverse mesh unfolding methods. An ellipsoidal model with 500 meshes is flattened by **(A)** Steepest edge unfolding, **(B)** Flat-Tree unfolding, and **(C)** the proposed Genetic Algorithm unfolding method, which is optimized to reduce the cut length. **(D-E)** By ignoring the crease lines of the flattened figure obtained from Steepest Edge unfolding, the computational wrapping concept is demonstrated with a paper for a 3D-printed ellipsoid. **(F)** An EL panel can also be attached on the ellipsoid without gaps and **(G)** can operate well without any failure. (Photo credit: Y.-K. Lee, Seoul National University)

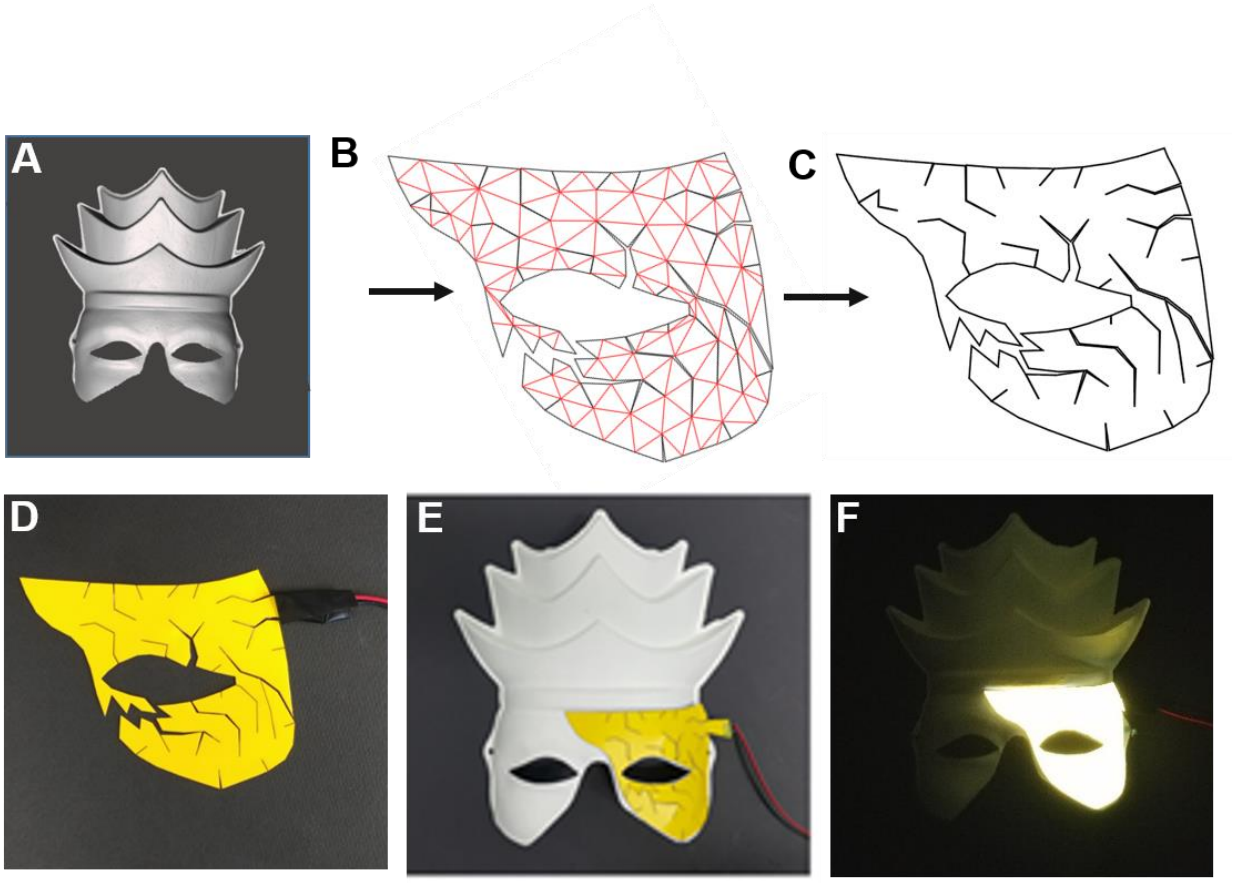

Fig. S7. Computational wrapping for a Korean facial mask. Traditional Korean masks can be covered with commercial EL panels. **(A)** The mask is 3D-scanned, and a complex part containing both positive and negative Gaussian curvatures is remeshed with 169 meshes. **(B)** That part is then mesh unfolded, and **(C)** the crease lines are ignored to apply our bending and attaching concept. **(D)** A commercial EL panel is cut with a laser cutter and **(E)** stably attached on the mask. **(F)** The light can be operated without failure, and the cut seams are blurred and invisible. (Photo credit: Y.-K. Lee, Seoul National University)

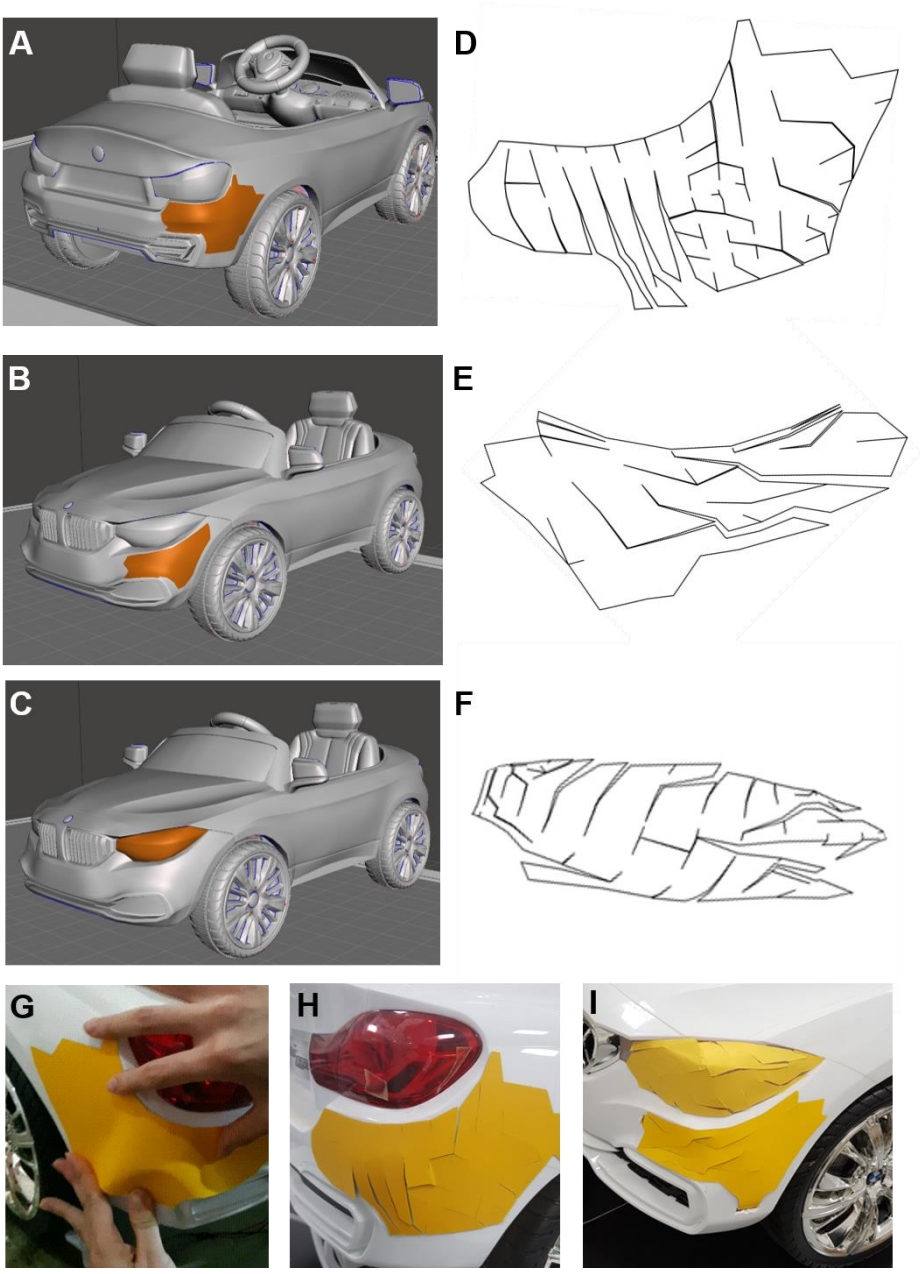

Fig. S8. Computational wrapping for curved vehicle exteriors. Meshes are generated for the nonzero Gaussian surfaces of an electric toy vehicle: **(A)** the edge of the rear side bumper, **(B)** the edge of the front side bumper, and **(C)** the headlights. Then, **(D-F)** the meshes are algorithmically unfolded with the GA unfolding method. Cuttable, nonstretchable, commercial EL lighting panels consisting of brittle electrodes are cut with a laser cutter to form the generated developable nets, which are attached to the electric toy vehicle with double-sided tape. **(G)** Without having the developable net, the rear side bumper region cannot be wrapped conformably, and spaces are left between the simple cut pattern and the vehicle surface. However, the developable nets **(H and I)** are conformably attached without gaps or overlapping, and the attached EL panels operate well without any electrical failure (See Movie S3). (Photo credit: Y.-K. Lee, Seoul National University)

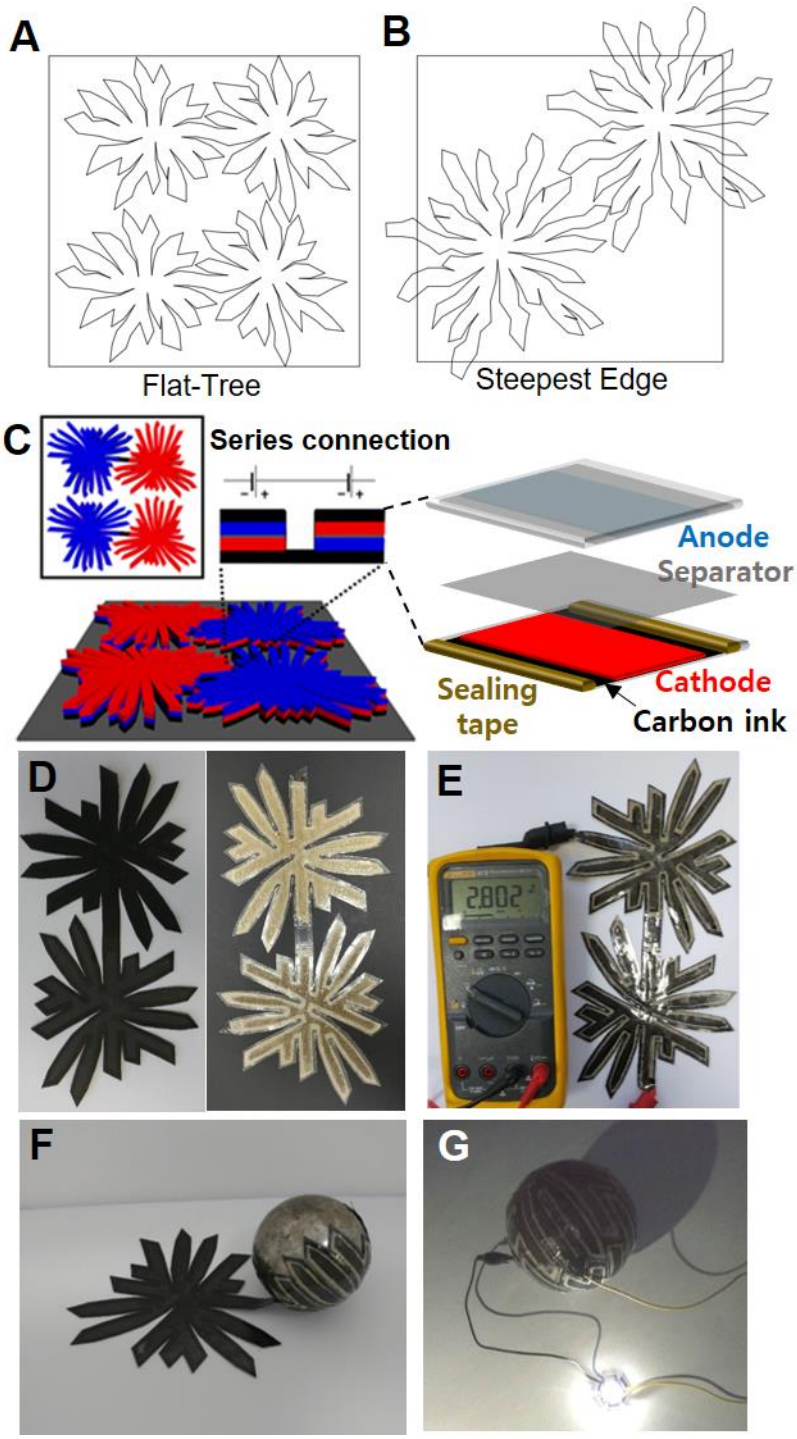

Fig. S9. Computational wrapping with a screen-printed flexible zinc-carbon primary battery. We fabricated a developable net of a primary battery for a sphere with a radius of 4 cm by using the screen printing method. Because the screen printing area is fixed at 30 cm × 30 cm, which is a geometric restriction of printing, the diversity of the developable net (See Fig. S3) can yield manufacturing advantages. For instance, **(A)** the Flat-Tree unfolding method generates a developable net where two radial patterns are connected through a strip and can be placed on the square printing area, whereas **(B)** the SE unfolding method generates a radial net pattern so that

two patterns cannot be placed on the square printing area at the same time. Since two developable nets can be placed on the printing area at the same time in the Flat-Tree unfolding method, this method produces less material waste than the SE unfolding method. **(C-D)** Furthermore, the developable net via the Flat-Tree method can have the advantage for the serial connection of batteries. Since the zinc-carbon primary battery can deliver 1.5 V of direct current, two cells should be serially connected to operate a light-emitting diode (LED) lamp that requires more than 1.5 V to operate. The Flat-Tree unfolding method generates a developable net with 180 meshes having two radial patterns connected through a strip. Two serially connected battery cells for 3.0 V can be fabricated at once. Current collector materials are printed on a developable net. The positive electrode materials are printed on one of the radial patterns of the developable net, and the negative electrode materials are printed on the other radial pattern of the developable net. On the strip connecting the two radial patterns, only the current collector is printed on one of the substrates. An electrolyte-soaked separator with a developable net is placed between the two electrodes, and finally, the two substrates are sealed together with double-sided tape. **(E)** The serially connected conformal Zn-carbon battery has a 2.8 open-circuit voltage. **(F)** This battery can stably wrap a steel ball and **(G)** can illuminate an LED lamp that requires more than 1.5 V to operate. We used 50 μm-thick polyethylene terephthalate (PET) films as substrates, conductive carbon grease as the current collector, MnO_2 and Zn powder-based slurry as electrodes, and a solution of 28 wt% $ZnCl_2$ and 3 wt% NH_4Cl in water for the electrolyte. Each MnO_2 and Zn powder-based slurry contains 5 wt% Super P carbon black, 2 wt% polyethylene oxide (PEO) powder, 1.5 wt% poly methyl methacrylate (PMMA) powder and 1.5 wt% polyvinyl pyrrolidone (PVP). (Photo credit: Y.-K. Lee, Seoul National University)

Movie S1
Failure to cover a sphere with nonstretchable sheets.

Movie S2
FE simulation for wrapping a sphere with a 100 μm-thick Si wafer with a nonpolyhedral developable net.

Movie S3
Demonstration of a conformable device with an electric toy car.

REFERENCES AND NOTES

1. C. Yang, Z. Suo, Hydrogel ionotronics. *Nat. Rev. Mater.* **3**, 125–142 (2018).

2. C.-C. Kim, H.-H. Lee, K. H. Oh, J.-Y. Sun, Highly stretchable, transparent ionic touch panel. *Science* **353**, 682–687 (2016).

3. S. Lin, S. Lin, H. Yuk, T. Zhang, G. A. Parada, H. Koo, C. Yu, X. Zhao, Stretchable hydrogel electronics and devices. *Adv. Mater.* **28**, 4497–4505 (2016).

4. J. A. Rogers, T. Someya, Y. Huang, Materials and mechanics for stretchable electronics. *Science* **327**, 1603–1607 (2010).

5. J. Y. Oh, S. Rondeau-Gagné, Y. C. Chiu, A. Chortos, F. Lissel, G. N. Wang, B. C. Schroeder, T. Kurosawa, J. Lopez, T. Katsumata, J. Xu, C. Zhu, X. Gu, W. G. Bae, Y. Kim, L. Jin, J. W. Chung, J. B. Tok, Z. Bao, Intrinsically stretchable and healable semiconducting polymer for organic transistors. *Nature* **539**, 411–415 (2016).

6. R. C. Webb, R. M. Pielak, P. Bastien, J. Ayers, J. Niittynen, J. Kurniawan, M. Manco, A. Lin, N. H. Cho, V. Malyrchuk, G. Balooch, J. A. Rogers, Thermal transport characteristics of human skin measured in vivo using ultrathin conformal arrays of thermal sensors and actuators. *PLOS ONE* **10**, e0118131 (2015).

7. L. Xu, S. R. Gutbrod, Y. Ma, A. Petrossians, Y. Liu, R. C. Webb, J. A. Fan, Z. Yang, R. Xu, J. J. Whalen III, J. D. Weiland, Y. Huang, I. R. Efimov, J. A. Rogers, Materials and fractal designs for 3D multifunctional integumentary membranes with capabilities in cardiac electrotherapy. *Adv. Mater.* **27**, 1731–1737 (2015).

8. T. C. Shyu, P. F. Damasceno, P. M. Dodd, A. Lamoureux, L. Xu, M. Shlian, M. Shtein, S. C. Glotzer, N. A. Kotov, A kirigami approach to engineering elasticity in nanocomposites through patterned defects. *Nat. Mater.* **14**, 785–789 (2015).

9. J. Stillwell, *Mathematics and Its History* (Springer Science & Business Media, 2010).

10. J. Hure, B. Roman, J. Bico, Wrapping an adhesive sphere with an elastic sheet. *Phys. Rev. Lett.* **106**, 174301 (2011).

11. Y. Cho, J.-H. Shin, A. Costa, T. A. Kim, V. Kunin, J. Li, S. Y. Lee, S. Yang, H. N. Han, I.-S. Choi, D. J. Srolovitz, Engineering the shape and structure of materials by fractal cut. *Proc. Natl. Acad. Sci. U.S.A.* **111**, 17390–17395 (2014).

12. M. Konaković, K. Crane, B. Deng, S. Bouaziz, D. Piker, M. Pauly, Beyond developable: Computational design and fabrication with auxetic materials. *ACM Trans. Graph.* **35**, 1–11 (2016).

13. M. P. Do Carmo, *Differential Geometry of Curves and Surfaces: Revised and Updated Second Edition* (Courier Dover Publications, 2016).

14. J. S. McCranie, *An Investigation of the Size of Epsilon-Nets* (University of Illinois, 1986).

15. E. D. D. a. J. O'Rourke, *Geometric Folding Algorithms* (Cambridge Univ. Press, 2007).

16. W. Schlickenrieder, "Nets of polyhedra," thesis, Technische Universität Berlin (1997).

17. D. Julius, V. Kraevoy, A. Sheffer, D-Charts: Quasi-developable mesh segmentation. *Comp. Graph. Forum* **24**, 581–590 (2005).

18. M. Bern, E. D. Demaine, D. Eppstein, E. Kuo, A. Mantler, J. Snoeyink, Ununfoldable polyhedra with convex faces. *Comput. Geom. Theory Appl.* **24**, 51–62 (2003).

19. Y.-H. K. Y. Hao, Z. Xi, J.-M. Lien, Creating foldable polyhedral nets using evolution control, in *Proceedings of the Robotics: Science and Systems* (2018).

20. Y.-H. K. Y. Hao, J.-M. Lien, Synthesis of fast and collision-free folding of polyhedral nets, in *Proceedings of the ACM Symposium on Computational Fabrication (SCF)* (2018).

21. Y.-H. Kim, Z. Xi, J.-M. Lien, Disjoint convex shell and its applications in mesh unfolding. *Comput. Aided Des.* **90,** 180–190 (2017).

22. Z. Xi, Y.-h. Kim, Y. J. Kim, J.-M. Lien, Learning to segment and unfold polyhedral mesh from failures. *Comput. Graph.* **58**, 139–149 (2016).

23. P. M. Dodd, P. F. Damasceno, S. C. Glotzer, Universal folding pathways of polyhedron nets. *Proc. Natl. Acad. Sci. U.S.A.* **115**, E6690-E6696 (2018).

24. S. Takahashi, H.-Y. Wu, S. H. Saw, C.-C. Lin, H.-C. Yen, Optimized topological surgery for unfolding 3D meshes. *Comput. Graph. Forum* **30**, 2077–2086 (2011).

25. X. Li, T. Kasai, S. Nakao, H. Tanaka, T. Ando, M. Shikida, K. Sato, Measurement for fracture toughness of single crystal silicon film with tensile test. *Sens. Act. A Phys.* **119**, 229–235 (2005).

26. F. Ericson, Schweitz J.-Å.. Micromechanical fracture strength of silicon. *J. Appl. Phys.* **68**, 5840–5844 (1990).

27. M. A. Mahmoud, A. Hosseini, Assessment of stress intensity factor and aspect ratio variability of surface cracks in bending plates. *Engineering fracture mechanics* **24**, 207–221 (1986).

28. J. H. Sung, J. H. Kim, R. H. Wagoner, A plastic constitutive equation incorporating strain, strain-rate, and temperature. *Int. J. Plast.* **26**, 1746–1771 (2010).

29. M. Safaei, M.-G. Lee, S.-l. Zang, W. De Waele, An evolutionary anisotropic model for sheet metals based on non-associated flow rule approach. *Comput. Mater. Sci.* **81**, 15–29 (2014).